Viscous dissipation in large amplitude oscillatory shear of unsaturated wet granular matter

Ahmad Awdi, Camille Chateau, Francois Chevoir, Jean-Noël Roux, Abdoulaye Fall

Viscous dissipation in large amplitude oscillatory shear of unsaturated wet granular matter

Ahmad Awdi,[1] Camille Chateau,[1] François Chevoir,[1] Jean-Noël Roux,[1] and Abdoulaye Fall[1]
Laboratoire NAVIER, UMR 8205-Université Gustave Eiffel, École des Ponts, CNRS, 77420 Champs-sur-Marne

(*Correspondence email address: abdoulaye.fall@cnrs.fr)

(Dated: 18 July 2024)

The present work investigates nonlinear behavior in large amplitude oscillatory shear (LAOS) of unsaturated wet granular materials using pressure-imposed rheometric measurements that enable to explore how the material properties characterizing the flow response depend on both strain amplitude and frequency of deformation. Away from the quasistatic limit, we show that the energy dissipated per unit volume in a single LAOS cycle, which can be visualized by the area enclosed by the Lissajous curve of stress versus strain, is an increasing function of the viscosity of the wetting liquid and is also influenced by the reduced pressure (comparing the cohesive to confining forces) and the frequency. Introducing the inertial number I and the viscous number I_v as previously done, it is shown that the influence of surface tension, viscosity, and driving frequency can be captured by plotting the dissipated energy per unit volume versus the viscous number: a good collapse is obtained. It is shown that an increase in liquid content shifts the whole curve of the dissipated energy upwards, indicating that the overall dissipation mechanism does not change with liquid content, only the energy dissipation related to the internal structure and its breakdown changes.

I. INTRODUCTION

In particulate systems, the addition of a liquid strongly modifies the mechanical/rheological properties. If the wet granular medium is not completely saturated, capillary forces can bring discrete particles together into a space network with a yield stress and the surface tension changes the elastic properties of the medium[1,2]. This is illustrated by the well known example of sand which, when wetted with small amounts of water, develops sufficient yield stress to allow construction of elaborate sand castles[3–6]. Static properties such as the tensile strength and the yield stress of a cohesive wet granular material are extremely sensitive to its preparation. Existing studies demonstrate that the angle of repose (angle below which the flow stops) and the angle of avalanches (angle above which a static assembly of grains flows) of a wet grain assembly initially increase with the liquid content, but afterward saturate[7–10] due to the fact that the cohesive stress between grains increases from zero and becomes constant rapidly, at a very low liquid content[11,12]. X-ray microtomographic images reveal that shear strength starts to increase when capillary bridges form between the grains. For increasing liquid content, the capillary bridges merge and eventually disappear when the granular media is fully saturated[1,13–15].

When the hydrodynamic forces are neglected, the rheology of these materials is characterized experimentally[12,15] and numerically[12,15,16] in terms of two dimensionless control parameters (we assumed the shear flow in direction 1 and the velocity gradient in direction 2): the inertial number $I = \dot{\gamma} d \sqrt{\rho/\sigma_{22}}$ which compares the inertial time scale of a particle of average size d and mass density ρ in a granular material submitted to a confining stress σ_{22} and the macroscopic shear deformation time scale $1/\dot{\gamma}$ of the granular material[17?] and the reduced pressure $P^* = \sigma_{22} d^2/F_0$ which compares confining forces $\sigma_{22} d^2$ to cohesive forces (at the grain scale) F_0[16]. Assuming that the contact angle of the liquid with the surface of the grain is small, F_0 can be approximated as $F_0 \simeq \pi \Gamma d$ for spherical grains of diameter d joined by menisci of surface tension Γ. Note that P^* is the inverse of the "cohesion number" which was defined in[9,18–20]. Thus, when $P^* \ll 1$, cohesive forces are dominant while the properties of cohesionless systems are retrieved in the limit of large P^*[12,16].

In fully saturated materials, i.e. suspensions, viscous forces are dominant. In such cases, the fluid affects granular flow by its viscosity η_f, and another dimensionless number called viscous number $I_v = \eta_f \dot{\gamma}/\sigma_{22}$, comparing viscous and confining stress, must be introduced[21–23] rather than inertial number I. In the limit of Stokes flow, as all inertia terms become negligible, the inertial number is irrelevant. However, in the presence of both inertial and viscous effects, constitutive laws and state parameters within the flowing material should depend on both I and I_v. Some authors proposed that both numbers should be combined into one single visco-inertial number which solely controls macroscopic stresses and micromorphology[20].

Furthermore, the elastic and viscous properties of cohesive wet granular materials are greatly influenced by the wetting liquid properties[1]. The purpose of this article is an experimental investigation of the influence of the viscosity η_f of the wetting liquid in the limit of small liquid content, called pendular regime, using large amplitude oscillatory shear (LAOS). LAOS measurements are useful for a large class of complex fluids because strain amplitude and frequency can be varied independently allowing a broad spectrum of conditions to be attained[24]. The description of the nonlinear material response has gained renewed interest and is subject of current research[24–27]. The variations of the complex moduli G' and G'' in LAOS as a function of liquid content and wetting liquid viscosity are measured. Away from the quasistatic limit, it is shown that the dissipation energy per unit volume in a single LAOS cycle, $E_d = \oint \sigma_{12}\, d\gamma$, which can be visualized by the area enclosed by the Lissajous curve of stress versus strain, is an increasing function of η_f and is also influenced by P^* and the driving frequency.

It is shown that the influence of surface tension, viscosity

and driving frequency can be captured by plotting the dissipated energy per unit volume versus the viscous number: a good collapse is obtained. It is shown that an increase in liquid content shifts the whole curve of the dissipated energy upwards, indicating that the overall dissipation mechanism does not change with liquid content, only the energy dissipation related to the internal structure and its breakdown changes.

II. EXPERIMENTAL METHODS

A. Materials

The experiments are carried out on model materials: slightly polydisperse assemblies of macroscopic solid spherical beads, mixed with a nonvolatile, wetting, Newtonian liquid. We use rigid polystyrene beads (Dynoseeds TS 500, Microbeads SA) of density $\rho = 1050 kg/m^3$ and of diameter $d = 0.5mm$ (with a standard deviation of 5%, sufficient to prevent crystallization). We always prepare the system before measurements in the same way to ensure reproducible experimental conditions: the wetting liquid is mixed thoroughly with the dry beads until a uniform consistency is visually obtained. To be able to vary the liquid viscosity, we use silicone oils. The viscosity η_f of silicone oils covers range $9-5535 mPas$ at $20^\circ C$ with surface tension $\Gamma = 20.4 \pm 0.2 mN/m$. Surface tension is measured with an automatic single drop tensiometer ($TRACKER^{TM}$, by *Teclis Scientific*). We define the liquid content as $\varepsilon = V_l/V_s$, where V_l and V_s, respectively denote the volumes of liquid and of solid beads. We prepare samples with a fixed liquid content: $\varepsilon = 0.015$, $\varepsilon = 0.05$ and $\varepsilon = 0.075$. A liquid content of $\varepsilon = 0.05$ is used unless indicated otherwise. Particular care is taken with the high-viscosity silicone oil, since it tends to form small binder-rich lumps.

B. Measurement apparatus and specifications

Granular materials must be confined to carry out rheometric experiments, and are conveniently characterized in shear flow under controlled normal stress[28]. Normal stress-imposed rheological measurements are carried out using a home-made annular shear device, as in our recent publications[12,15,29]. The annulus-shaped cell containing the grains is limited by smooth cylindrical walls in the radial direction, and to avoid wall slip, both the rotating and vertically mobile upper boundary and the static lower substrate are serrated, with $0.5mm$ ridges to which the grains may fit. The inner and outer radii of the annular cell are $R_i = 21$ and $R_o = 45mm$ (thus $R_i/R_o \approx 0.4$, and the width of the annular trough is about $48d$). The filling height h of the annular box is adjustable from a few (typically 5) to 100 particle diameters. Oscillatory shear experiments under confining pressure are carried out using a stress-controlled rheometer (Anton Paar MCR 502).

C. Measurements

Before each measurement, the sample is poured into the shear cell and compacted, at $20^\circ C$, by imposing a normal force of $10N$ under $1Hz$ oscillation cycle with an angular displacement of π; allowing thus a good filling of the annular shear cell. In such case, the solid packing fraction reached at this initial stage is $\phi_0 = 0.6 \pm 0.005$ (for most of the experiments). LAOS experiments were performed then under a stress-controlled mode with an imposed normal force. Indeed, instead of setting the value of the gap size for a given experiment, we impose the normal force and then, under oscillatory shear, we let the gap size h vary in order to maintain the desired value of the normal force[29]. We then have access to instantaneous measurements of the torque and the gap variation for imposed normal force and strain. In this case, the solid volume fraction ϕ_S is not fixed but adjusts to the imposed strain. Since the sample is allowed to dilate, the liquid content ε as defined here is rigorously constant under measurements in contrast to the saturation number $S = \frac{\varepsilon \phi_S}{1-\phi_S}$.

In oscillatory rheology, both the elastic and viscous properties of a material can be examined simultaneously by applying an oscillatory strain $\gamma(t) = \gamma_0 \sin(\omega t)$ which automatically imposes a strain rate $\dot{\gamma}(t) = \gamma_0 \omega \cos(\omega t)$. The resulting oscillatory shear stress $\sigma_{12}(t, \omega, \gamma_0)$ is recorded and analyzed. Here, ω is the applied angular oscillation frequency (rad/s), γ_0 is the strain amplitude, and t is the time. In contrast to small amplitude oscillatory shear ($\gamma_0 \ll 1$) where the relation between applied stress and induced shear is assumed to be linear, the large amplitude regime is characterized by a nonlinear response of the system when γ_0 exceeds some critical value. Oscillatory strain amplitude sweeps, at different frequencies (0.1, 1, 2, and $3Hz$), allow probing the sample at a fixed time scale $t = 1/\omega$, while the strain amplitude γ_0 is continuously increased during a $15min$ logarithmic ramp from 10^{-6} to 1678. Dynamic storage G' and loss G'' moduli are, hence, measured as a function of the strain amplitude γ and the frequency ω.

Table I lists all the parameter values for the experiments conducted.

Parameters	Range
$\eta_f(mPas)$	9, 20, 53, 111, 350, 1095, 5535
$\varepsilon(-)$	0.015, 0.03, 0.05, 0.075
$P^*(-)$	1, 2.3, 4.6, 6.9, 9.3
$f(Hz)$	0.1, 1, 2, 3
$\gamma(-)$	10^{-6}-1678

TABLE I. List and ranges of the parameters conducted

We have checked that the phase angle for all measurements is less than 100° meaning that instrumental inertia is negligible[30].

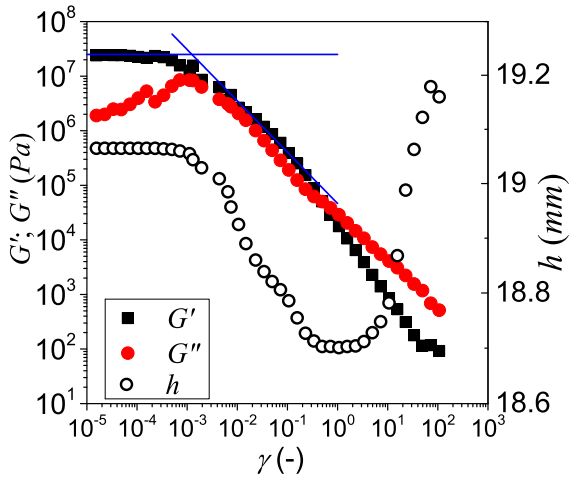

FIG. 1. Typical measurements of the dynamic moduli G', G'' (the left axis) and of the gap size variation h (the right axis) as a function of strain amplitude γ at a frequency of $1Hz$ for a viscosity $\eta_f = 9mPas$ and a reduced pressure $P^* = 2.3$. Blue lines are the power-law fittings of the behaviors of G' well-above and well-below the strain crossover.

III. RESULTS

Figure 1 shows storage G' and loss G'' moduli as a function of the strain amplitude γ for $\eta_f = 9mPas$ and $\omega = 1Hz$. For small strain amplitude, moduli are independent of the applied strain amplitude and G' is always larger than G'', which corresponds to a linear viscoelastic behavior and elastic domination. Then, for intermediate strain, the dynamic moduli decrease with a constant slope, and for larger strain, a crossover ($G' \leq G''$) is observed, meaning that the viscous contribution then dominates the elastic one, which indicates that the material flows.

We denote by γ_c the strain crossover and by γ_L the limit of the linear regime, defined as the intersection of the power law equations fitting the behaviors of G' well-above and well-below γ_c (cf. Fig.1)[31]. Figures 2 a and b show that γ_L and γ_c strongly increase when the reduced pressure P^* increases. Notice that γ_L and γ_c are only functions of P^*.

An estimate of shear modulus G'_e in the linear regime may be obtained as in Ref.[32]. G'_e, in bead assemblies with Hertzian contacts, is of the order of the bulk modulus B_e. B_e is itself correctly approximated (especially for large coordination numbers, near 6 or above), in cohesionless bead assemblies under pressure P, by the Voigt estimate B_e^V. Depending on coordination number z, and on modulus E^* (defined as $E^* = \dfrac{2}{1-\nu^2}$, E and ν denoting, respectively, the Young modulus and the Poisson ratio of the material the beads are made of). This estimate is given by

$$B_e^V = \frac{1}{2}\left(\frac{z\phi_S E^*}{3\pi}\right)^{2/3} P^{1/3}. \qquad (1)$$

Due to cohesive forces pressing the grains onto their neighbors, pressure P, in Eq. 1 should be replaced by the *effective pressure*[12], and one should use

$$P = \sigma_{22} + \frac{\bar{z}\phi_S F_0}{\pi d^2}. \qquad (2)$$

In this relation, coordination number $\bar{z}$ counts the contacts and the menisci joining noncontacting grains, weighted by ratio F/F_0 of the attractive force to its maximum (contact) value F_0[12], and may be approximated as $(z+z_t)/2$ if z_t is the total coordination number. This effect of attractive forces on elastic moduli through an effective pressure was recognized in [33,34].

A typical value of G'_e/B_e^V in isotropic assemblies of spherical beads with large coordination numbers (near 6) is 1.1[32]. Contact network anisotropy, which could affect this ratio, is presumably small under oscillatory shear of small amplitude. In Fig. 2c, the estimated value

$$G'_e = 1.1 \times B_e^V, \qquad (3)$$

using relations 1 and 2, is shown to provide correct estimates of G'_e. It is evaluated with $E^* = 4.10^9$ Pa (adequate for polystyrene), and values $z = 5.5$, $\bar{z} = 6.5$ (nearly independent of P^*) as obtained in the simulations of Ref.[12] (which agreed quantitatively with the experiments with the same beads as used in the present study).

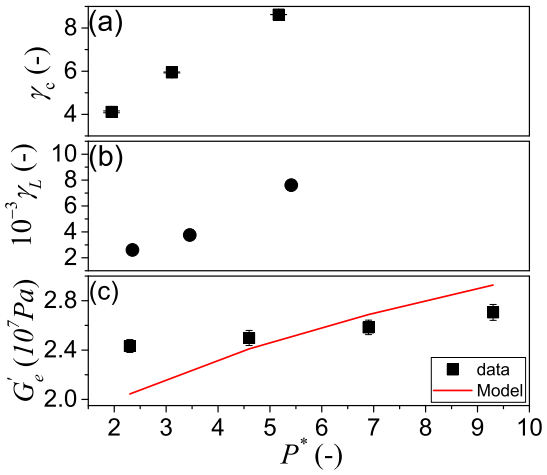

FIG. 2. Variation of γ_L (b), γ_c (a), and G'_e (c) with reduced pressure for $\eta_f = 9mPas$. (c) also displays predicted values of G'_e, using Eq. 3.

During a shear cycle, the gap size h is not fixed but adjusts to the imposed strain as shown in Fig. 1. In the linear regime, h remains constant, then decreases for intermediate strains before increasing when $\gamma \geq \gamma_c$. The decrease/increase in the gap size corresponds to the continuous compaction/dilation of the material under strain. Under a fixed normal pressure, the granular packing first compacts before dilating into a final critical state for sufficient strain[29]. Since particles cannot escape from the shear cell, $\phi_S \propto h^{-1}$[15]. The minimum value h_0 corresponds to the maximum solid packing fraction ϕ_c: shearing necessarily implies immediate dilatancy of the granular media. Notice

that during a loop in an oscillatory measurement, the rheometer software shows only the mean value of the recorded gap size and not its evolution.

These results suggest that low strain could cause a strongly nonlinear response for unsaturated wet granular material. Such behavior is qualitatively similar to that observed in yield stress materials and is attributed to the pendular network and to the dissipation of the frictional contact of the grains under confinement[35].

Increasing P^* induces a denser, stiffer contact network which requires a higher strain to be broken and initiate the flow. Thus, the strain crossover γ_c, for which the wet granular media expands to accommodate its deformation may be interpreted in terms of the microstructural breakdown of the menisci.

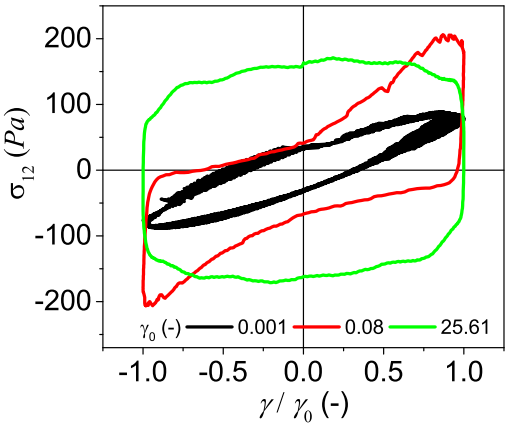

FIG. 3. Lissajous curves: Total stress $\sigma_{12}(t)$ versus normalized strain $\gamma(t)/\gamma_0$ at $f = 1Hz$, $P^* = 2.3$ and $\eta_f = 9mPas$ for three values of γ_0.

Lissajous $\sigma_{12}(\gamma)$ curves, in which the total stress is plotted parametrically against the total strain, were then used to relate the response of the sample to the imposed oscillatory strain. In this representation, a linear viscoelastic response is characterized by an ellipse, symmetric with respect to the line $\sigma_{12} = \gamma$. The two limiting cases of purely elastic and purely viscous response are characterized by a line and a circle, respectively[36]. At sufficient small strain amplitude, i.e. 0.1%, the Lissajous curve is an ellipse and the area of the Lissajous tends to be very small. For an intermediate strain amplitude, nonlinear behavior is already evident in the Lissajous curve (Fig. 3), which is not elliptical anymore. The area encompassed by the curve increases. An elastic deformation is then observed leading to a linear increase in stress. The nonlinear response occurs as the saturation of the stress signal initiates the yielding process[37,38]. The stress increases continuously as the strain increases further, reaching the absolute value of maximum stress. This overshoot in the stress curve is due to yielding of the sample, and afterwards the sample begins to flow[39]. For much larger γ_0, the curves get broader indicating further increasing dissipation and increasing nonlinearity. For $\gamma_0 = 25.61$, which is larger than γ_c, the shape of the Lissajous curves changed to an almost rectangular shape and approached the behavior of an idealized Bingham model[40].

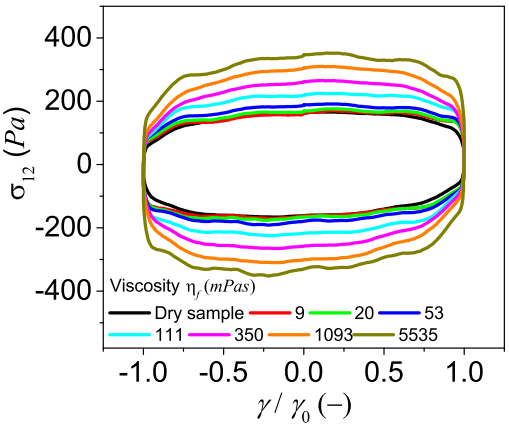

FIG. 4. Lissajous curves: solid lines are total stress $\sigma_{12}(t)$ versus normalized strain $\gamma(t)/\gamma_0$. $\gamma_0 = 25.61$, $f = 1Hz$, $P^* = 2.3$; different wetting liquid viscosity. Noticed that the dry data overlap the low-viscosity wet data at a high strain rate (i.e. at $\gamma \approx 0$) since viscous effect is negligible here. However, near the flow reversal, the small differences between wet and dry come from the cohesion due to the addition of the wetting liquid.

In Fig. 3, the area enclosed in the Lissajous curve can be interpreted as the energy dissipated per unit volume $E_d = \oint \sigma_{12}\, d\gamma$ during one complete cycle of the oscillatory strain that is imposed. Over the range tested, E_d strongly increases when the viscosity η_f increases as shown in Fig. 4 and in Fig. 5. This last figure also shows that E_d strongly increases when the reduced pressure P^* increases in the nonlinear viscoelastic regime.

The dissipated energy gives a physical interpretation to the Lissajous curve and presents an alternative way to review the flow behavior of the material. For unsaturated wet granular materials, E_d takes into account both the inertia of the grains (energy is lost due to inelasticity and friction when grains collide or slide past each other) and the viscous dissipation of the wetting liquid. Thus, in order to isolate the effects of the wetting liquid alone, the dissipated energy per unit volume is measured under the same conditions on the dry granular material and is called E_0. Figure 5 reveals that normalizing E_d with E_0 gives a master curve, whatever the reduced pressure P^*.

Moreover, an increase in liquid content shifts the whole curve of the dissipated energy upwards as shown in Fig. 6, indicating that, (in the pendular regime), the overall dissipation mechanism does not change with liquid content, only the energy dissipation related to the internal structure and its breakdown changes since the inter-grain cohesive force is proportional to the number of capillary liquid bridges. Indeed, it is known from x-ray microtomography[13] that the number of capillary bridges per grain depends of the liquid content: it increases rapidly at low ε before saturating at intermediate liquid contents; then, when the liquid content increases further, it drastically vanishes to the detriment of dimers, trimers

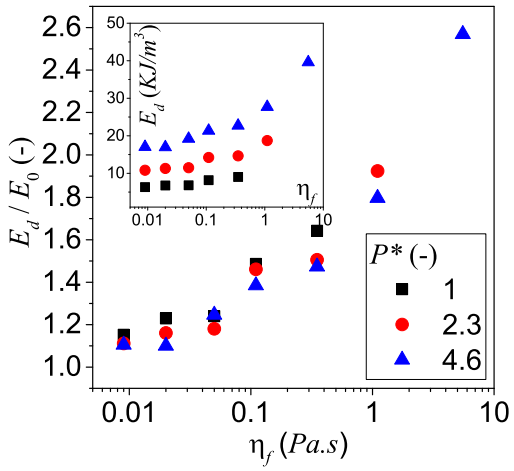

FIG. 5. Normalized dissipated energy per unit volume E_d/E_0 vs viscosity η_f for different reduced pressure P^*. E_0 corresponds to the dissipated energy per unit volume of the dry sample under the same conditions. The inset shows the dissipated energy per unit volume E_d versus viscosity at different P^*.

and larger liquid/grain clusters[13,15].

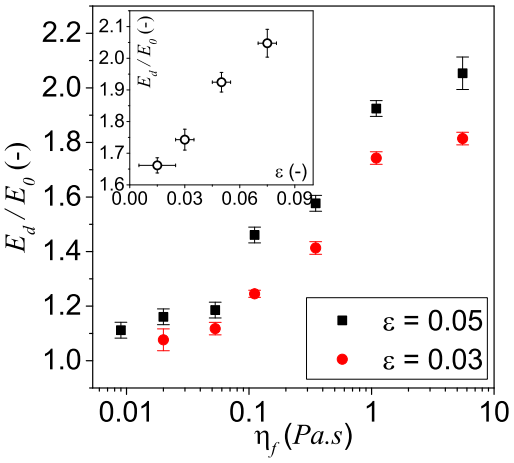

FIG. 6. Normalized dissipated energy per unit volume E_d/E_0 vs viscosity η_f at $P^* = 2.3$ for two liquid contents. Inset: E_d/E_0 vs the liquid content for $\eta_f = 1Pas$ and $P^* = 2.3$.

To provide a further qualitative analysis of the nonlinear rheology of unsaturated granular materials under LAOS, the dependence of the normalized dissipated energy per unit volume with viscosity for four typical driving frequencies is shown in Fig. 7 at a given $P^* = 2.3$. Figure 7 shows that E_d/E_0 increases when the driving frequency ω increases, whatever the viscosity of the wetting liquid, and that this behavior is further strengthened as the shear strain amplitude increases.

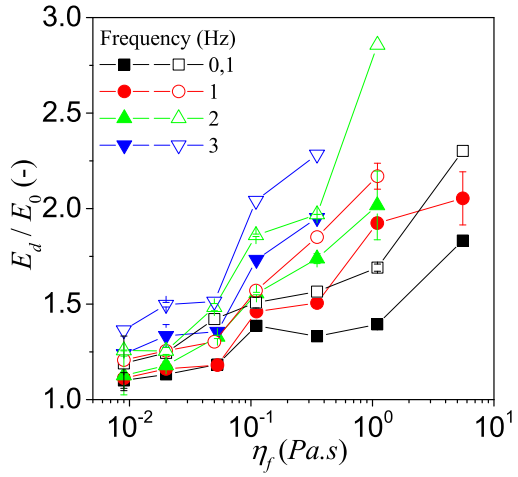

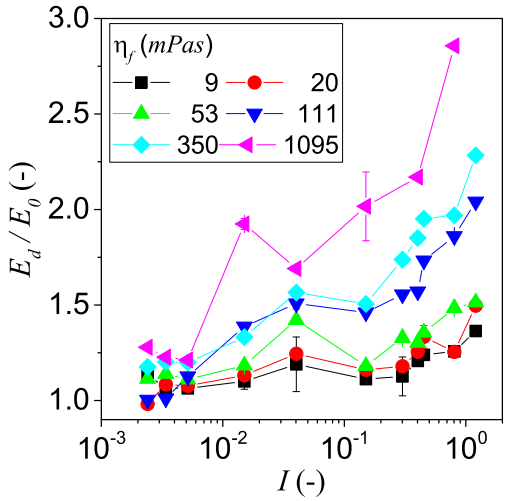

FIG. 7. a) Normalized energy per unit volume E_d/E_0 vs viscosity η_f for different imposed frequency. The closed symbols are for $\gamma_0 = 25.61$ and the open symbols are for $\gamma_0 = 68.2$. b)Normalized energy per unit volume E_d/E_0 vs inertial number I for different viscosities η_f at $P^* = 2.3$.

In order to analyze our results in the frame of $\mu(I)$-rheology[17,41], we define an inertial number such as

$$I = \gamma_0 \omega \sqrt{\frac{\rho d^3}{\pi \Gamma P^*}} \tag{4}$$

Figure 7b shows how E_d/E_0 vary throughout the flow regimes. Notice that for these data points, the inertia number varies from 0.0024 to 1.2 which covers quasistatic and dense flow regimes. Thus, for low inertial number, the normalized dissipated energy per unit volume tends to a finite value, which is strongly influenced by capillary forces: it increases with increasing P^* (data not shown). When the inertial number is increased, E_d/E_0 increases whatever the viscosity of the wetting liquid.

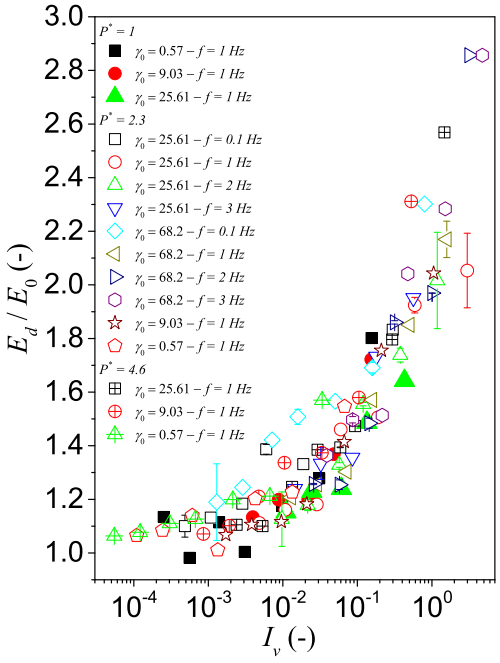

FIG. 8. E_d/E_0 vs the viscous number I_v for different imposed frequency f, different γ_0 and different reduced pressure P^*.

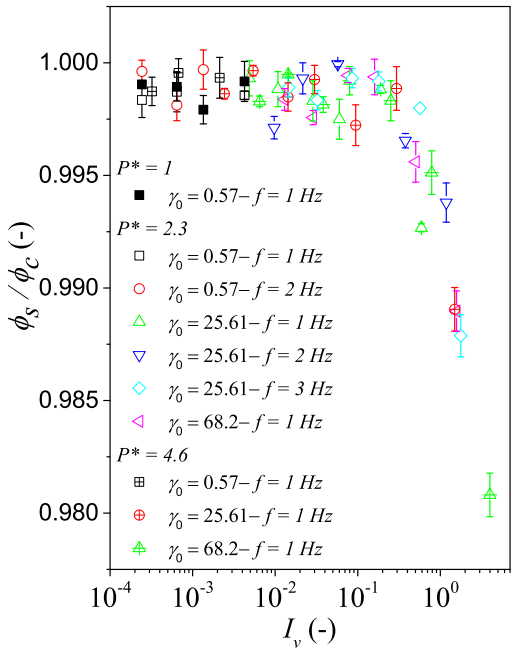

FIG. 9. Dimensionless solid packing fraction ϕ_S/ϕ_c vs the viscous number I_v for different imposed frequency f, different γ_0 and different reduced pressure P^*.

The reason for those dependencies can be attributed to the rate-dependent relaxation of the microstructure since in faster flows, deformation rates of liquid bridges introduce varied shear rates in the fluids, causing viscous flow in the liquid menisci. Consequently the system is no longer governed by the inertial number. To evidence that, we introduce the viscous number I_v calculated as

$$I_v = \frac{\eta_f \omega \gamma_0 d}{\pi \Gamma P^*} \tag{5}$$

As predicted, the plot of E_d/E_0 versus I_v evidence a collapse of experimental data points onto a single curve (Fig. 8. A comparison of Figs. 7b and 8 indicates that I_v, rather than I, is the relevant parameter. Moreover, the plot clearly divides into two regions: for low viscous number, the dimensionless dissipated energy per unit volume is roughly constant, independent of I_v. This shows that in this region, dynamic viscous effects are negligible. When the viscous number increases further, E_d/E_0 increases with increasing viscous number revealing that in this region, viscous forces are significant/dominant. Notice that as defined here, I and I_v are the maximum value of the inertial and the viscous number, respectively, under the cycle.

We turn now to the gap variation as seen in Fig. 1, i.e. the dynamical dilatancy that describes the variation of the solid packing fraction ϕ_S under LAOS measurements. In Fig. 9, the normalized solid packing fraction ϕ_S/ϕ_c is plotted as a function of the viscous number I_v. Once again, all the data points collapse on a single curve. At low I_v, ϕ_S/ϕ_c is quasi-constant. When I_v increases, the inertia starts influencing the flow and the system becomes rate dependent: the ratio ϕ_S/ϕ_c decreases; this regime corresponds to the dense flow in which the granular material dilates.

IV. CONCLUSION

This paper outlines the importance of studying the LAOS properties of unsaturated wet granular materials under controlled confining stress conditions. The main conclusions are as follows:

-When the deformation exceed the crossover strain γ_c i.e away from the quasi-static regime, the dissipation energy E_d increases with the fluid viscosity η_f and is influenced by the reduced pressure P^* and the oscillation frequency ω. We have shown that E_d is an increasing function of P^* for the explored range of viscosity, and by increasing the driving frequency, E_d/E_0 increases whatever the viscosity of the wetting liquid. Such behavior was further strengthened as the shear strain amplitude increased.

-By changing the liquid content, the dissipation energy curve is shifted upwards suggesting that the overall dissipation mechanism does not change but that the energy dissipation related to the evolution of the internal structure changes.

- A good collapse of the experimental data is obtained by plotting the normalized dissipated energy per unit volume versus the viscous number I_v, indicating that, in the explored parameter range, I_v rather than the inertial number I is the control parameter that captures simultaneously the influence of surface tension, viscosity and driving oscillation frequency.

One of the original aspect of the paper is the investigation of the influence of the viscosity of the wetting liquid in the limit of small liquid content on the energy dissipated using large amplitude oscillatory shear (LAOS). While the results shown in Figs. 8 and 9 are quite promising, one may wish to explore to what extent they are sensitive to the spatial distribution of the liquid phase, that is supposed to be homogeneous. Moreover, it would be interesting to introduce the extended $\mu(I)$-rheology recently proposed[15] in the determination of the dissipated energy E_d. Indeed, knowing this rheology, it is then possible to write the momentum balance of the unsaturated granular layer during an oscillatory strain amplitude sweeps under confining stress: $\sigma_{12} = \mu^* \sigma_{22}$ where $\mu^* = \mu_0^* + \alpha I_v$ with μ_0^* being the friction coefficient in the quasistatic regime[12]. Doing so, one predicts that, in the quasistatic regime, the dissipated energy evolves with the confining pressure as $E_d = 4\mu_0^* \gamma_0 \sigma_{22}$. This is indeed observed and the corresponding μ_0^* values are in perfect agreement with those obtained experimentally and numerically in[12,15]. We should now extend our finding to the dense flow regime.

ACKNOWLEDGEMENTS

We are grateful to David Hautemayou and Cédric Mézière for technical help with the measurements. Funding from Agence Nationale de la Recherche within the frame of the national program Investments for the Future ANR-11-LABX-022-01 and also the project "RheoGranoSat" - ANR-16-CE08-0005-01 is gratefully acknowledged.

AUTHOR CONTRIBUTION STATEMENT

A.A. carried out the experiments, implementing methods supplied by A.F. A.A. and A.F. prepared the figures in their final form. A.F. and A.A. wrote the paper, which was thoroughly reviewed by F.C., J.-N.R. and C.C.

[1] A. Fall, B. Weber, M. Pakpour, N. Lenoir, N. Shahidzadeh, J. Fiscina, C. Wagner, and D. Bonn, "Sliding friction on wet and dry sand," Physical review letters **112**, 175502 (2014).

[2] M. Aliasgari, N. Maleki-Jirsaraei, and S. Rouhani, "The effect of liquid viscosity on sliding friction coefficient of wet granular materials," in *EPJ Web of Conferences*, Vol. 249 (EDP Sciences, Powders and Grains, 2021) p. 08003.

[3] R. Albert, I. Albert, D. Hornbaker, P. Schiffer, and A.-L. Barabási, "Maximum angle of stability in wet and dry spherical granular media," Physical Review E **56**, R6271 (1997).

[4] A.-L. Barabási, R. Albert, and P. Schiffer, "The physics of sand castles: maximum angle of stability in wet and dry granular media," Physica A: Statistical Mechanics and its Applications **266**, 366–371 (1999).

[5] T. C. Halsey and A. J. Levine, "How sandcastles fall," Physical Review Letters **80**, 3141 (1998).

[6] M. Pakpour, M. Habibi, P. Møller, and D. Bonn, "How to construct the perfect sandcastle," Scientific reports **2**, 1–3 (2012).

[7] S. Nowak, A. Samadani, and A. Kudrolli, "Maximum angle of stability of a wet granular pile," Nature Physics **1**, 50–52 (2005).

[8] L. Bocquet, E. Charlaix, and F. Restagno, "Physics of humid granular media," Comptes Rendus Physique **3**, 207–215 (2002).

[9] S. T. Nase, W. L. Vargas, A. A. Abatan, and J. McCarthy, "Discrete characterization tools for cohesive granular material," Powder Technology **116**, 214–223 (2001).

[10] L. Bocquet, E. Charlaix, S. Ciliberto, and J. Crassous, "Moisture-induced ageing in granular media and the kinetics of capillary condensation," Nature **396**, 735–737 (1998).

[11] V. Richefeu, M. S. El Youssoufi, and F. Radjai, "Shear strength properties of wet granular materials," Physical Review E **73**, 051304 (2006).

[12] M. Badetti, A. Fall, F. Chevoir, and J.-N. Roux, "Shear strength of wet granular materials: macroscopic cohesion and effective stress," The European Physical Journal E **41**, 1–16 (2018).

[13] M. Scheel, R. Seemann, M. Brinkmann, M. Di Michiel, A. Sheppard, B. Breidenbach, and S. Herminghaus, "Morphological clues to wet granular pile stability," Nature materials **7**, 189–193 (2008).

[14] J.-F. Bruchon, J.-M. Pereira, M. Vandamme, N. Lenoir, P. Delage, and M. Bornert, "Full 3d investigation and characterisation of capillary collapse of a loose unsaturated sand using x-ray ct," Granular Matter **15**, 783–800 (2013).

[15] M. Badetti, A. Fall, D. Hautemayou, F. Chevoir, P. Aimedieu, S. Rodts, and J.-N. Roux, "Rheology and microstructure of unsaturated wet granular materials: Experiments and simulations," Journal of rheology **62**, 1175–1186 (2018).

[16] S. Khamseh, J.-N. Roux, and F. Chevoir, "Flow of wet granular materials: a numerical study," Physical Review E **92**, 022201 (2015).

[17] F. Da Cruz, S. Emam, M. Prochnow, J.-N. Roux, and F. Chevoir, "Rheophysics of dense granular materials: Discrete simulation of plane shear flows," Physical Review E **72**, 021309 (2005).

[18] P. G. Rognon, J.-N. Roux, M. Naaim, and F. Chevoir, "Dense flows of cohesive granular materials," Journal of Fluid Mechanics **596**, 21–47 (2008).

[19] N. Berger, E. Azéma, J.-F. Douce, and F. Radjai, "Scaling behaviour of cohesive granular flows," EPL (Europhysics Letters) **112**, 64004 (2016).

[20] T. T. Vo, S. Nezamabadi, P. Mutabaruka, J.-Y. Delenne, and F. Radjai, "Additive rheology of complex granular flows," Nature communications **11**, 1–8 (2020).

[21] C. Cassar, M. Nicolas, and O. Pouliquen, "Submarine granular flows down inclined planes," Physics of fluids **17**, 103301 (2005).

[22] M. Trulsson, B. Andreotti, and P. Claudin, "Transition from the viscous to inertial regime in dense suspensions," Physical review letters **109**, 118305 (2012).

[23] L. Amarsid, J.-Y. Delenne, P. Mutabaruka, Y. Monerie, F. Perales, and F. Radjai, "Viscoinertial regime of immersed granular flows," Physical Review E **96**, 012901 (2017).

[24] K. Hyun, M. Wilhelm, C. O. Klein, K. S. Cho, J. G. Nam, K. H. Ahn, S. J. Lee, R. H. Ewoldt, and G. H. McKinley, "A review of nonlinear oscillatory shear tests: Analysis and application of large amplitude oscillatory shear (laos)," Progress in Polymer Science **36**, 1697–1753 (2011).

[25] D. Merger, *Large amplitude oscillatory shear investigations of colloidal systems: Experiments and constitutive model predictions*, Ph.D. thesis, Karlsruhe, Karlsruher Institut für Technologie (KIT), Diss., 2015 (2015).

[26] E. Y. Ong, M. Ramaswamy, R. Niu, N. Y. Lin, A. Shetty, R. N. Zia, G. H. McKinley, and I. Cohen, "Stress decomposition in laos of dense colloidal suspensions," Journal of Rheology **64**, 343–351 (2020).

[27] A. J. Sandoval, M. Fernández, O. Sanz, A. Santamaría, E. Penott-Chang, and A. J. Müller, "Large amplitude oscillatory shear (laos) behavior of chocolates of different compositions," Journal of Rheology **66**, 859–879 (2022).

[28] F. Boyer, É. Guazzelli, and O. Pouliquen, "Unifying suspension and granular rheology," Physical review letters **107**, 188301 (2011).

[29] A. Fall, G. Ovarlez, D. Hautemayou, C. Mézière, J.-N. Roux, and F. Chevoir, "Dry granular flows: Rheological measurements of the μ (i)-rheology," Journal of rheology **59**, 1065–1080 (2015).

[30] G. Yazar, O. Caglar Duvarci, M. Yildirim Erturk, and J. L. Kokini, "Laos (large amplitude oscillatory shear) applications for semisolid foods," in *Rheology of Semisolid Foods*, edited by H. S. Joyner (Springer International

Publishing, Cham, 2019) pp. 97–131.
[31]F. Rouyer, S. Cohen-Addad, and R. Höhler, "Is the yield stress of aqueous foam a well-defined quantity?" Colloids and Surfaces A: Physicochemical and Engineering Aspects **263**, 111–116 (2005).
[32]I. Agnolin and J.-N. Roux, "Internal states of model isotropic granular packings. iii. elastic properties," Physical Review E **76**, 061304 (2007).
[33]P. C. Møller and D. Bonn, "The shear modulus of wet granular matter," EPL (Europhysics Letters) **80**, 38002 (2007).
[34]H. Alarcon, J.-C. Géminard, and F. Melo, "Effect of cohesion and shear modulus on the stability of a stretched granular layer," Physical Review E **86**, 061303 (2012).
[35]F. Gorlier, Y. Khidas, A. Fall, and O. Pitois, "Optimal strengthening of particle-loaded liquid foams," Physical Review E **95**, 042604 (2017).
[36]R. H. Ewoldt, P. Winter, J. Maxey, and G. H. McKinley, "Large amplitude oscillatory shear of pseudoplastic and elastoviscoplastic materials," Rheologica acta **49**, 191–212 (2010).
[37]S. A. Rogers, B. M. Erwin, D. Vlassopoulos, and M. Cloitre, "Oscillatory yielding of a colloidal star glass," Journal of Rheology **55**, 733–752 (2011).
[38]K. van der Vaart, Y. Rahmani, R. Zargar, Z. Hu, D. Bonn, and P. Schall, "Rheology of concentrated soft and hard-sphere suspensions," Journal of Rheology **57**, 1195–1209 (2013).
[39]J. D. Park and S. A. Rogers, "The transient behavior of soft glassy materials far from equilibrium," Journal of Rheology **62**, 869–888 (2018).
[40]S. A. Rogers and M. P. Lettinga, "A sequence of physical processes determined and quantified in large-amplitude oscillatory shear (laos): Application to theoretical nonlinear models," Journal of rheology **56**, 1–25 (2012).
[41]G. M. gdrmidi@ polytech. univ-mrs. fr http://www. lmgc. univ-montp2. fr/MIDI/, "On dense granular flows," The European Physical Journal E **14**, 341–365 (2004).